Supporting information

New Visible-Light-Driven H_2- and O_2-Evolving Photocatalysts Developed by Ag(I) and Cu(I) Ion Exchange of Various Layered and Tunneling Metal Oxides Using Molten Salts Treatments

Kenta Watanabe[1], Katsuya Iwashina[1], Akihide Iwase[1,2], Shunsuke Nozawa[3], Shin-ichi Adachi[3], and Akihiko Kudo*[1,2]

[1]Department of Applied Chemistry, Faculty of Science, Tokyo University of Science, 1-3 Kagurazaka, Shinjuku-ku, Tokyo 162-8601, Japan

[2]Photocatalysis International Research Center, Research Institute for Science and Technology, Tokyo University of Science, 2641 Yamazaki Noda-shi, Chiba-ken 278-8510, Japan

[3]Institute of Materials Structure Science, High Energy Accelerator Research Organization, 1-1 Oho, Tsukuba, Ibaraki 305-0801, Japan

Contents

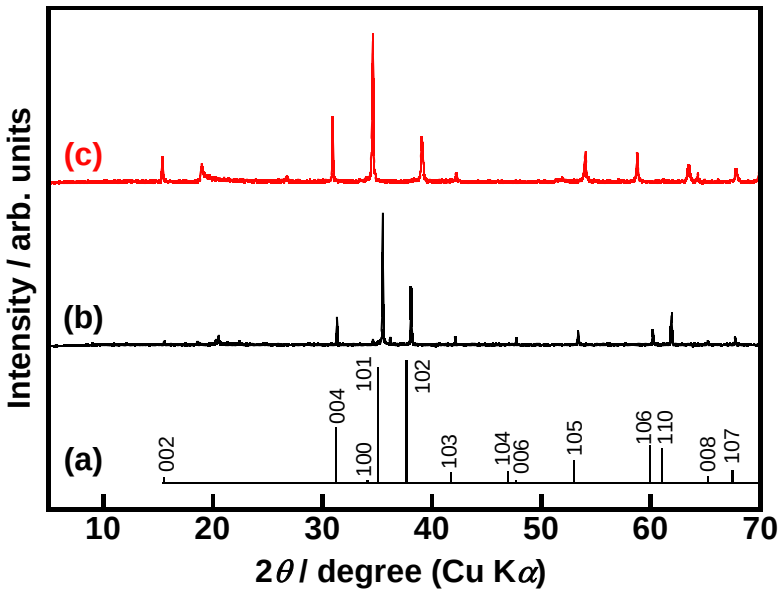

Figure S1. XRD patterns of (a) $CuFeO_2$ (Hexagonal, PDF 1-79-1546), (b) $CuLi_{1/3}Ti_{2/3}O_2$ (Hexaconal), and (c) Cu(I)-Li_2SnO_3. CuCl was used as a flux for the synthesis of $CuLi_{1/3}Ti_{2/3}O_2$ and Cu(I)-Li_2SnO_3.

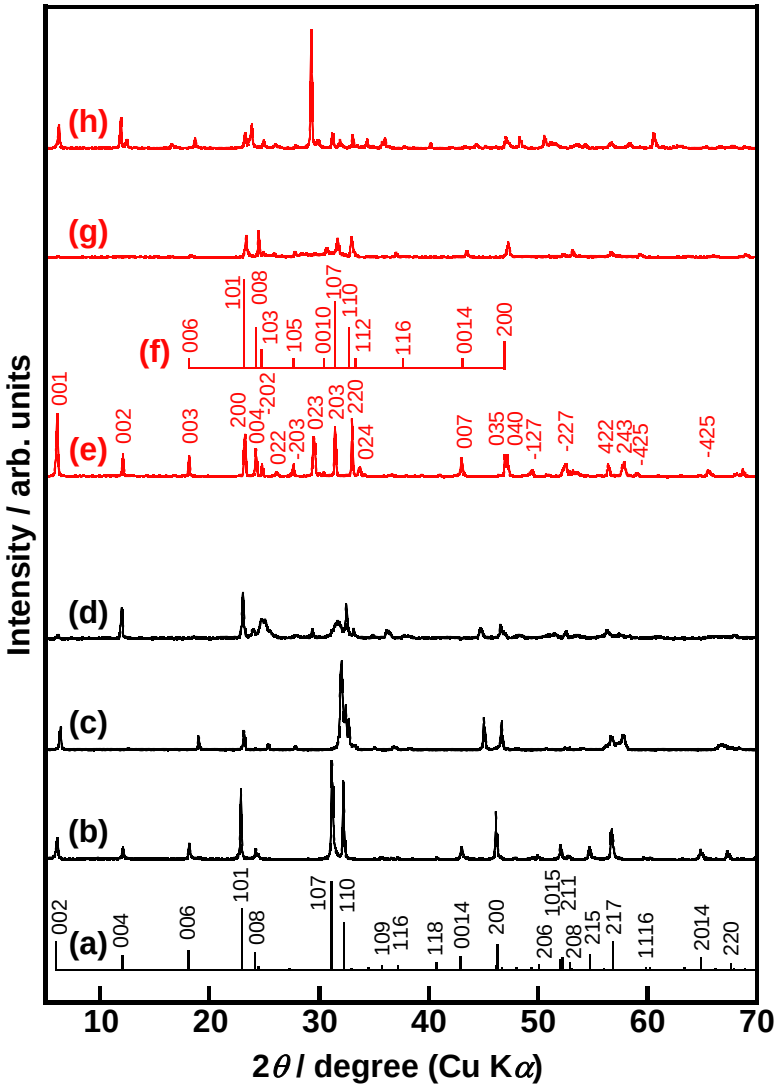

Figure S2. XRD patterns of (a) $K_2CaNaTa_3O_{10}$ (PDF 1-70-6006), (b) $K_2CaNaNb_3O_{10}$, (c) Ag(I)-$K_2CaNaNb_3O_{10}$, (d) Cu(I)-$K_2CaNaNb_3O_{10}$, (e) $KCa_2Nb_3O_{10}$, (f) $AgCa_2Ta_3O_{10}$ (PDF 52-1081), (g) Ag(I)-$KCa_2Nb_3O_{10}$, and (h) Cu(I)-$KCa_2Nb_3O_{10}$. CuCl was used as a flux for the synthesis of all Cu(I)-substituted materials. A plane index for $KCa_2Nb_3O_{10}$ was referred to PDF 1-75-9853.

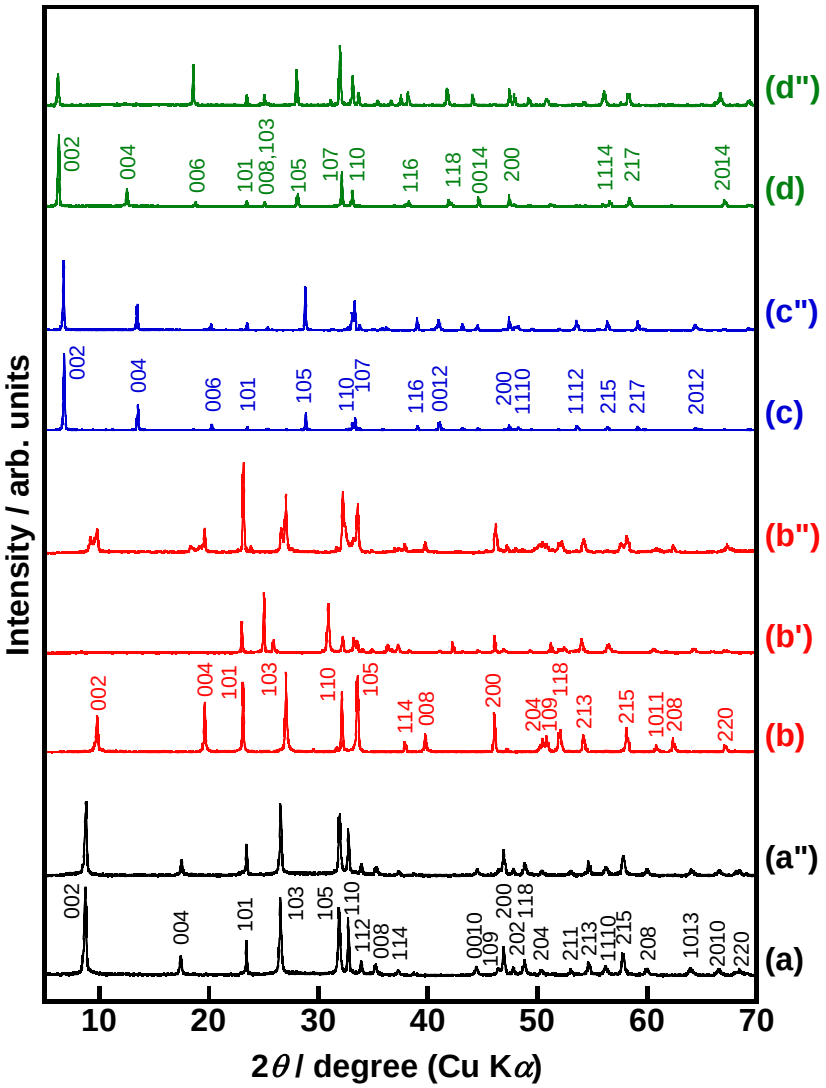

Figure S3. XRD patterns of layered metal oxides with and without molten salt treatments. Host materials, and their Ag(I)- and Cu(I)-ion-exchanged materials were labeled as (x), (x'), and (x"), respectively. (a) $LiLaTa_2O_7$, (b) $Li_2SrTa_2O_7$, (c) $Li_2La_2Ti_3O_{10}$, and (d) $Na_2La_2Ti_3O_{10}$. CuCl was used as a flux for the synthesis of all Cu(I)-substituted materials. Plane indices for $LiLaTa_2O_7$, $Li_2SrTa_2O_7$, $Li_2La_2Ti_3O_{10}$, and $Na_2La_2Ti_3O_{10}$ were referred to PDFs 1-82-8704, 1-89-8144, 1-87-1169, and 1-86-1369, respectively.

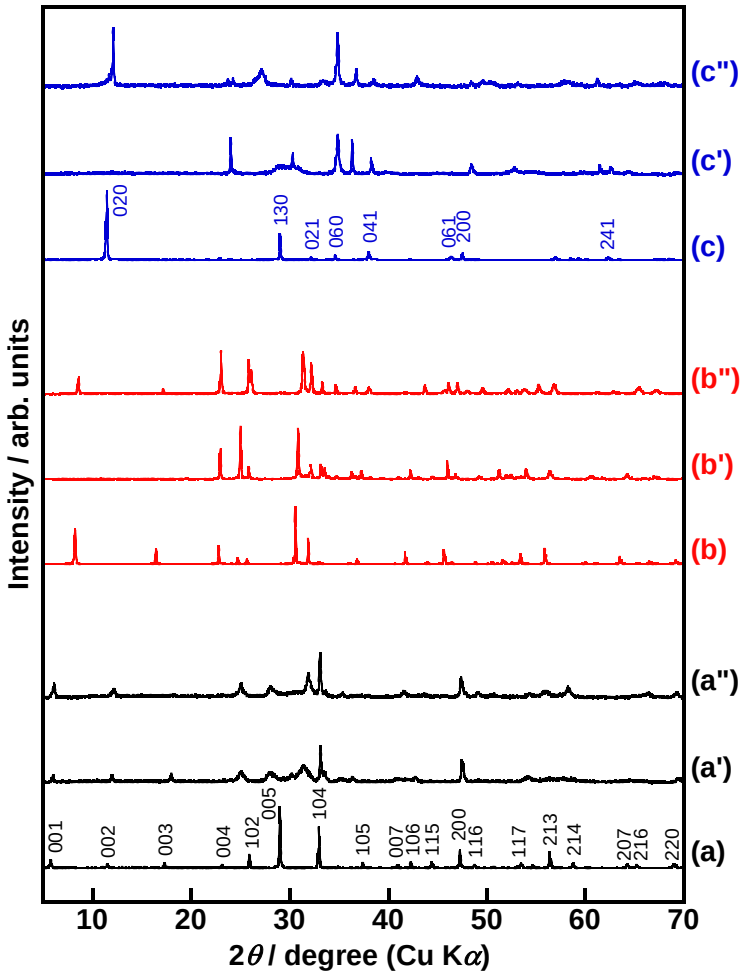

Figure S4. XRD patterns of layered metal oxides with and without molten salt treatments. Host materials, and their Ag(I)- and Cu(I)-ion-exchanged materials were labeled as (x), (x'), and (x"), respectively. (a) $CsLa_2Ti_2TaO_{10}$, (b) $K_2SrNb_{0.2}Ta_{1.8}O_7$, and (c) $K_{0.8}Mg_{0.4}Ti_{1.6}O_4$. CuCl was used as a flux for the synthesis of Cu(I)-$CsLa_2Ti_2TaO_{10}$ and Cu(I)-$K_2SrNb_{0.2}Ta_{1.8}O_7$. CuCl-CuI mixture was used as a flux for the synthesis of Cu(I)-$K_{0.8}Mg_{0.4}Ti_{1.6}O_4$. Plane indices for $CsLa_2Ti_2TaO_{10}$ and $K_{0.8}Mg_{0.4}Ti_{1.6}O_4$ were referred to PDFs 1-70-7828 and 1-73-671, respectively.

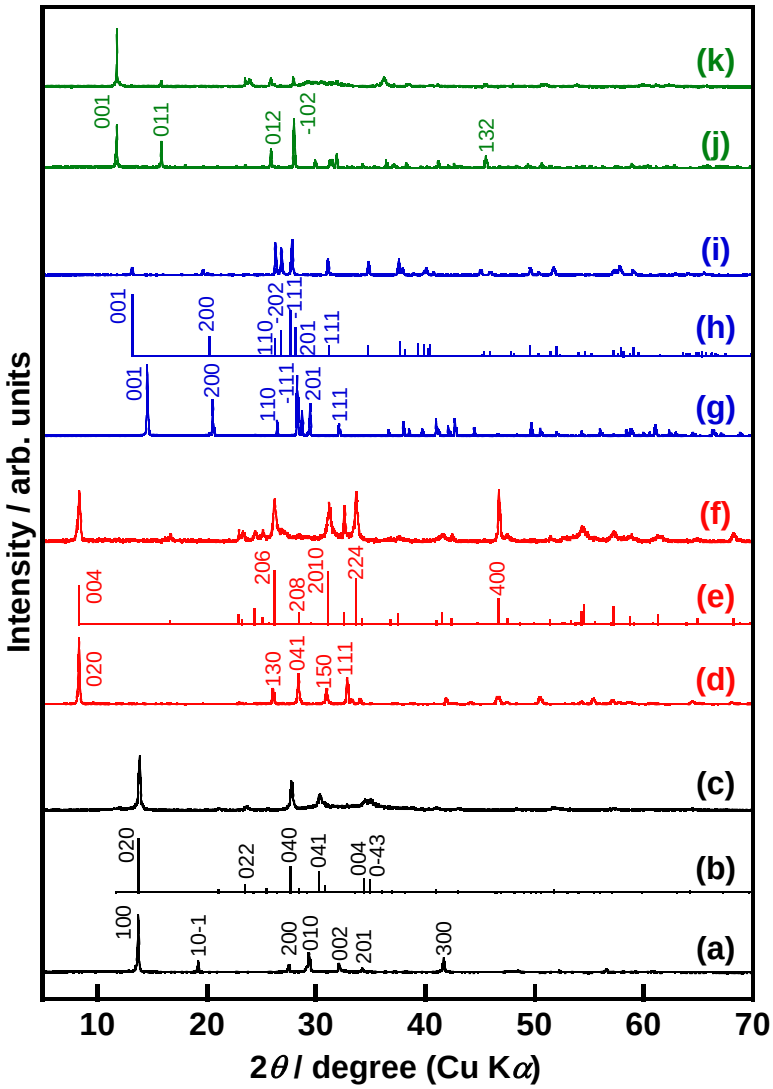

Figure S5. XRD patterns of (a) $K_2Ti_2O_5$, (b) $Ag_2Ti_2O_5$ (PDF: 56-131), (c) Ag(I)-$K_2Ti_2O_5$, (d) $KLaNb_2O_7$, (e) β-$AgLaNb_2O_7$ (PDF: 1-82-14), (f) Ag(I)-$KLaNb_2O_7$, (g) $LiVWO_6$, (h) $NaVWO_6$ (PDF: 1-79-5682), (i) Ag(I)-$LiVWO_6$, (j) KV_3O_8, and (k) Ag(I)-KV_3O_8. Plane indices for $K_2Ti_2O_5$, $KLaNb_2O_7$, $LiVWO_6$, and KV_3O_8 were referred to PDFs 51-1890, 1-81-1191, 1-78-5901, and 1-86-2495, respectively.

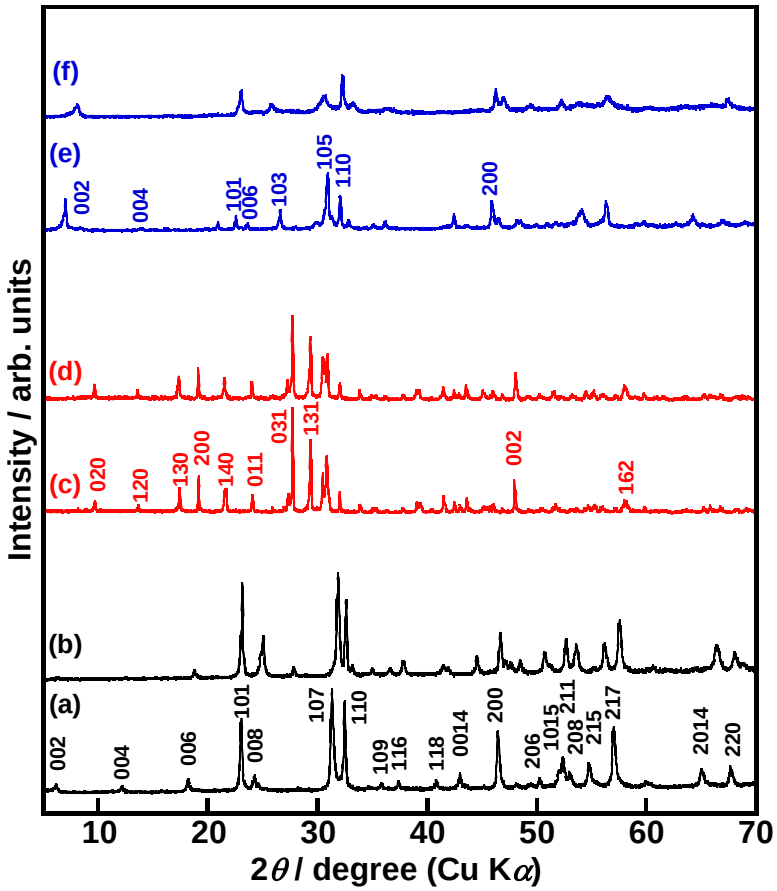

Figure S6. XRD patterns of (a) $K_2CaNaTa_3O_{10}$, (b) Cu(I)-$K_2CaNaTa_3O_{10}$, (c) $CsTi_2NbO_7$, (d) Cu(I)-$CsTi_2NbO_7$, (e) $K_2La_{2/3}Ta_2O_7$, and (f) Cu(I)-$K_2La_{2/3}Ta_2O_7$. CuCl was used as a flux for the synthesis of Cu(I)-$K_2CaNaTa_3O_{10}$ and Cu(I)-$K_2La_{2/3}Ta_2O_7$. CuCl-CuI was used as a flux for the synthesis of Cu(I)-$CsTi_2NbO_7$. Plane indices for $K_2CaNaTa_3O_{10}$, $K_2La_{2/3}Ta_2O_7$, and $CsTi_2NbO_7$ were referred to PDF 1-70-6006, 1-72-5958, and 1-73-680, respectively.

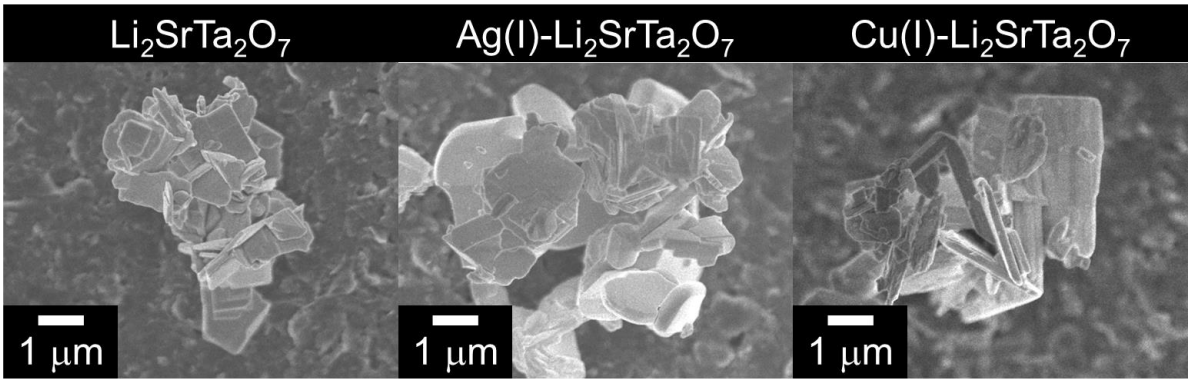

Figure S7. SEM images of $Li_2SrTa_2O_7$, Ag(I)-$Li_2SrTa_2O_7$, and Cu(I)-$Li_2SrTa_2O_7$.

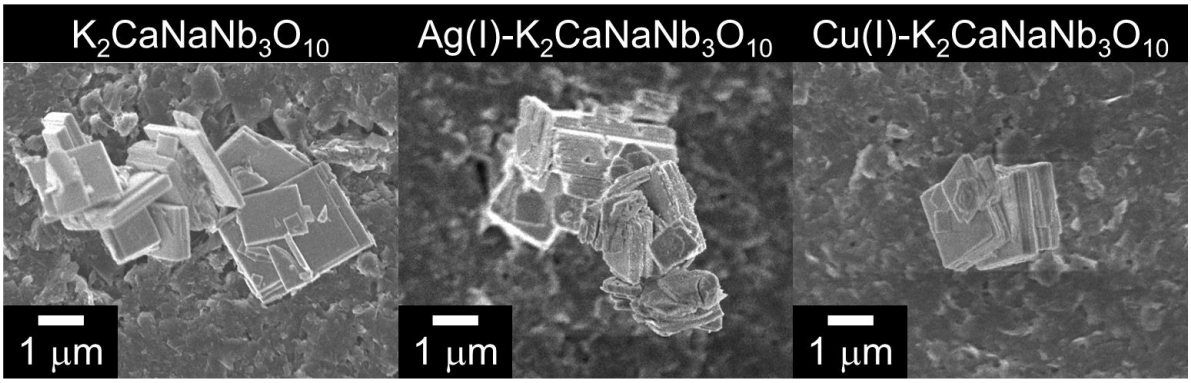

Figure S8. SEM images of $K_2CaNaNb_3O_{10}$, Ag(I)-$K_2CaNaNb_3O_{10}$, and Cu(I)-$K_2CaNaNb_3O_{10}$.

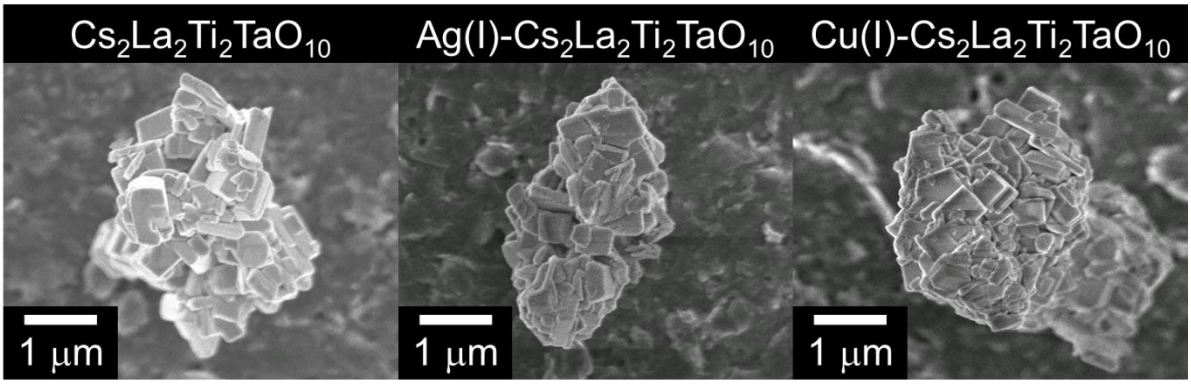

Figure S9. SEM images of $Cs_2La_2Ti_2TaO_{10}$, Ag(I)-$Cs_2La_2Ti_2TaO_{10}$, and Cu(I)-$Cs_2La_2Ti_2TaO_{10}$.

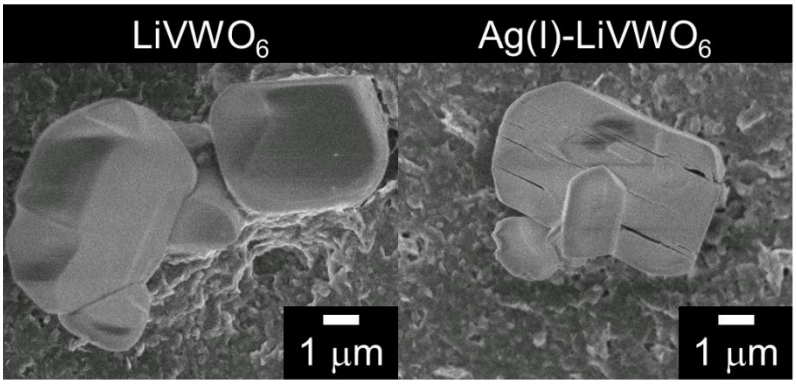

Figure S10. SEM images of $LiVWO_6$ and Ag(I)-$LiVWO_6$.

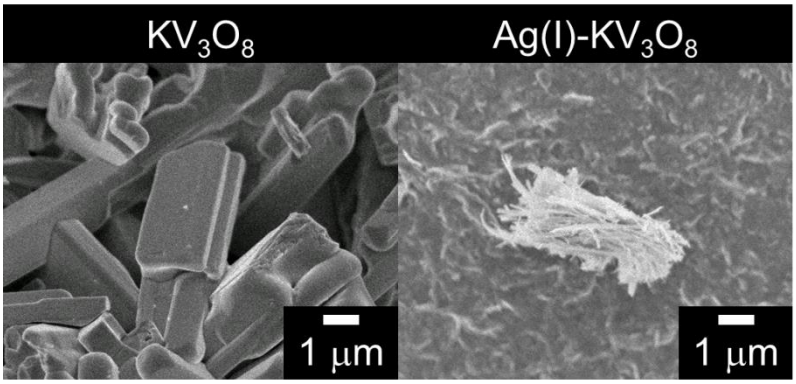

Figure S11. SEM images of KV_3O_8 and Ag(I)-KV_3O_8.

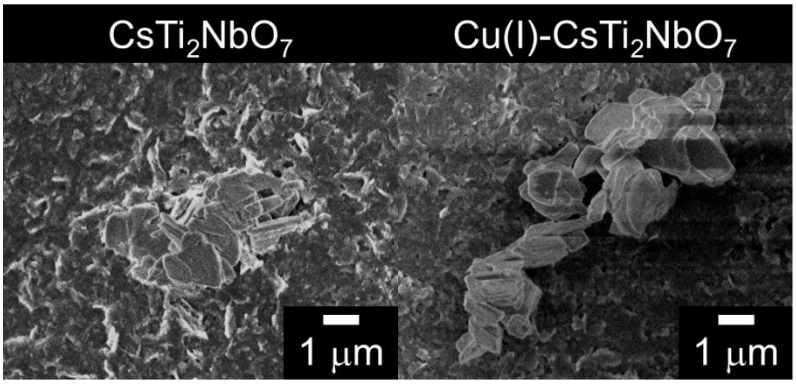

Figure S12. SEM images of $CsTi_2NbO_7$ and Cu(I)-$CsTi_2NbO_7$.

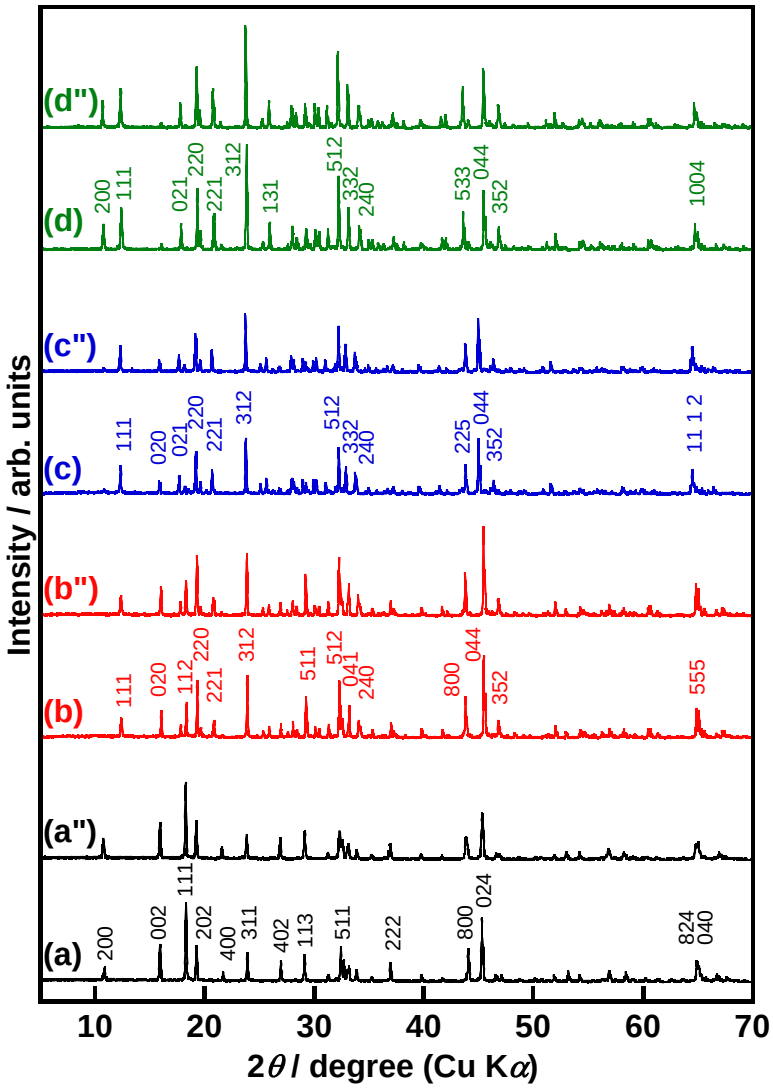

Figure S13. XRD patterns of metal oxides possessing a tunneling structure with and without molten salt treatments. Host materials and their Cu(I)-ion-exchanged materials were labeled as (x) and (x"), respectively. (a) $Li_2Na_2Ti_6O_{14}$, (b) $Li_2SrTi_6O_{14}$, (c) $Li_2BaTi_6O_{14}$, and (d) $Li_2PbTi_6O_{14}$. CuCl-CuI mixture was used as a flux for the synthesis of all Cu(I)-substituted materials. Plane indices for $Li_2Na_2Ti_6O_{14}$, $Li_2SrTi_6O_{14}$, $Li_2BaTi_6O_{14}$, and $Li_2PbTi_6O_{14}$ were referred to PDFs 52-690, 1-72-6072, 1-74-8154, and 1-74-8153, respectively.

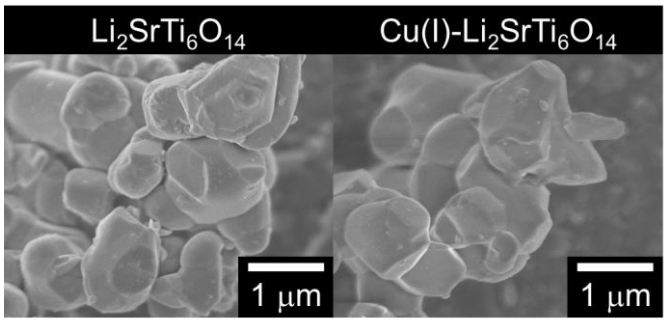

Figure S14. SEM images of $Li_2SrTi_6O_{14}$ and Cu(I)-$Li_2SrTi_6O_{14}$.

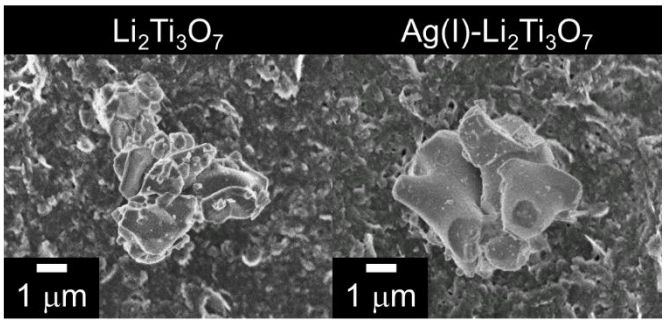

Figure S15. SEM images $Li_2Ti_3O_7$ and Ag(I)-$Li_2Ti_3O_7$.

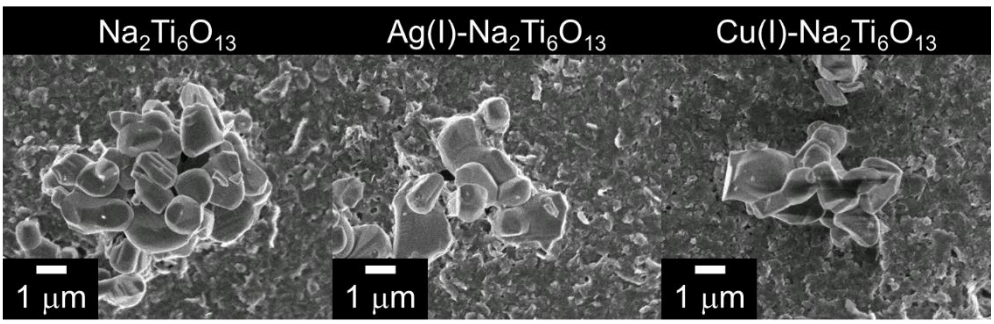

Figure S16. SEM images of $Na_2Ti_6O_{13}$, Ag(I)-$Na_2Ti_6O_{13}$, and Cu(I)-$Na_2Ti_6O_{13}$.

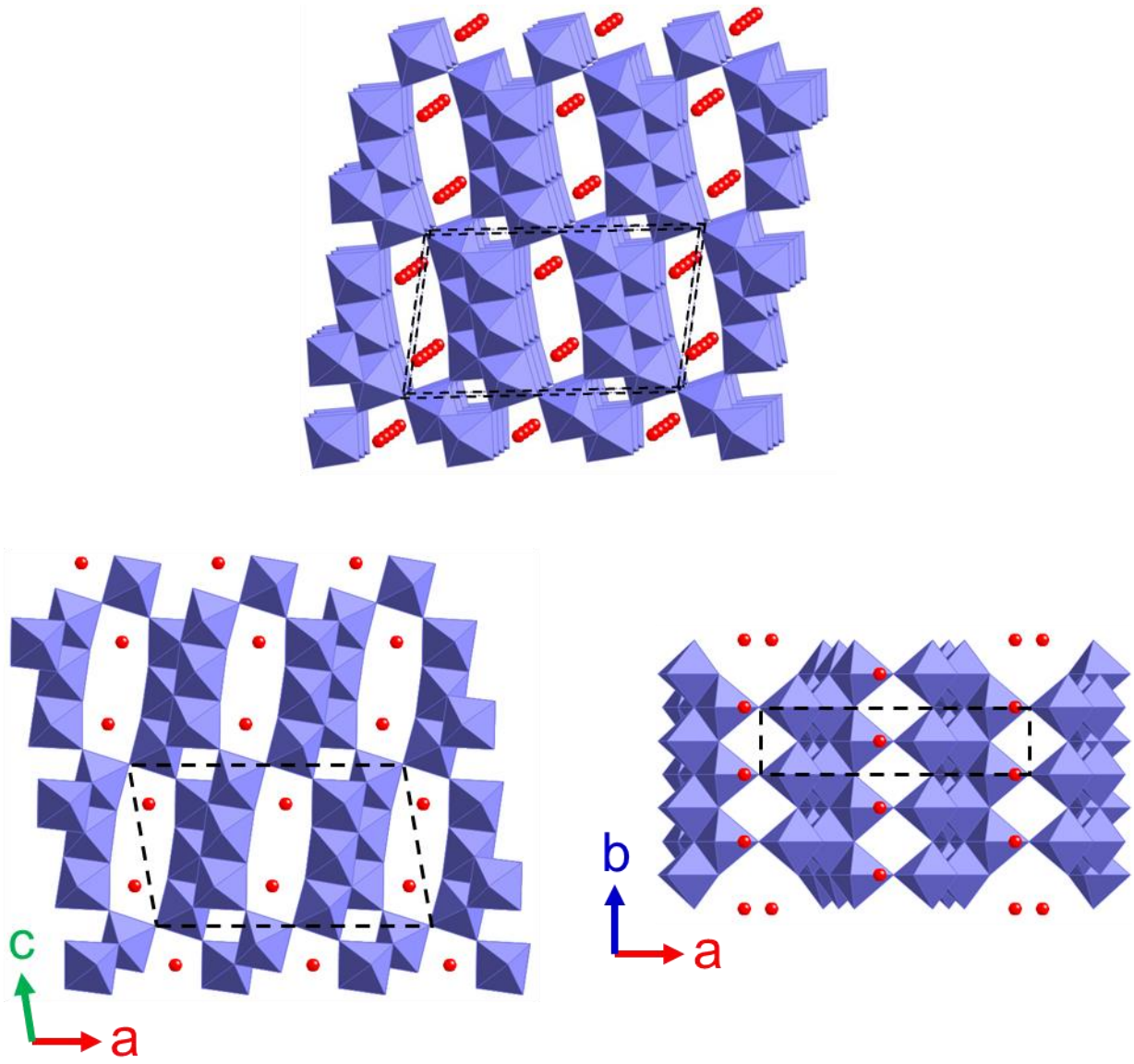

Figure S17. Crystal structure of $Li_2Ti_6O_{13}$ with a tunneling structure. Red spheres and blue octahedra indicate Li^+ and TiO_6, respectively.

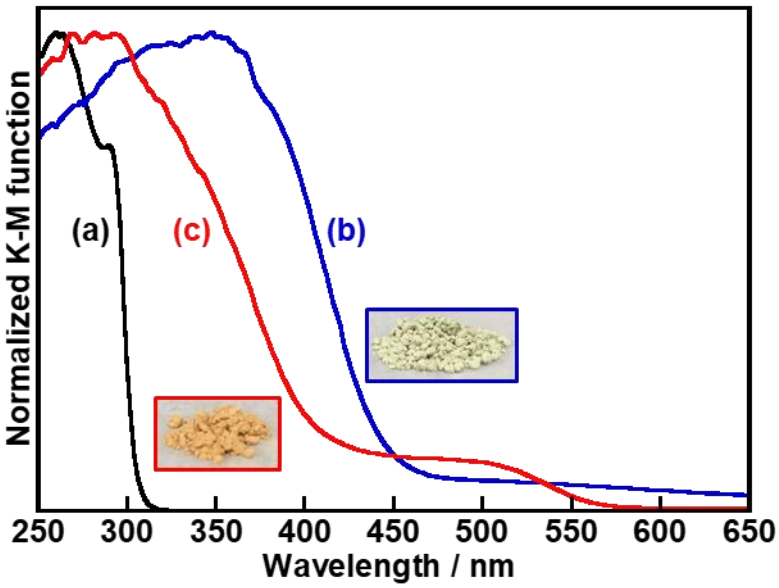

Figure S18. Diffuse reflectance spectra of (a) $Li_2SrTa_2O_7$, (b) Ag(I)-$Li_2SrTa_2O_7$, and (c) Cu(I)-$Li_2SrTa_2O_7$, and photographs of Ag(I)-$Li_2SrTa_2O_7$ (red frame) and Cu(I)-$Li_2SrTa_2O_7$ (blue frame).

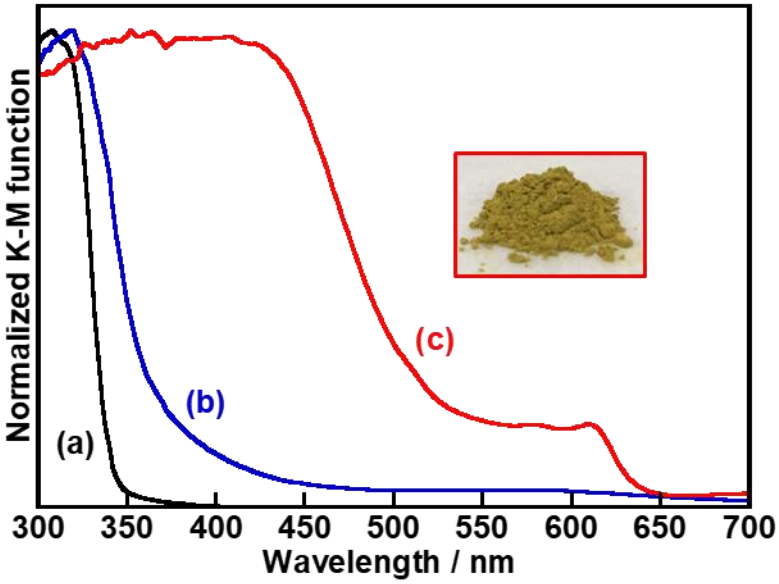

Figure S19. Diffuse reflectance spectra of (a) $K_2La_2Ti_3O_{10}$, (b) Ag(I)-$K_2La_2Ti_3O_{10}$, and (c) Cu(I)-$K_2La_2Ti_3O_{10}$, and a photograph of Cu(I)-$K_2La_2Ti_3O_{10}$.

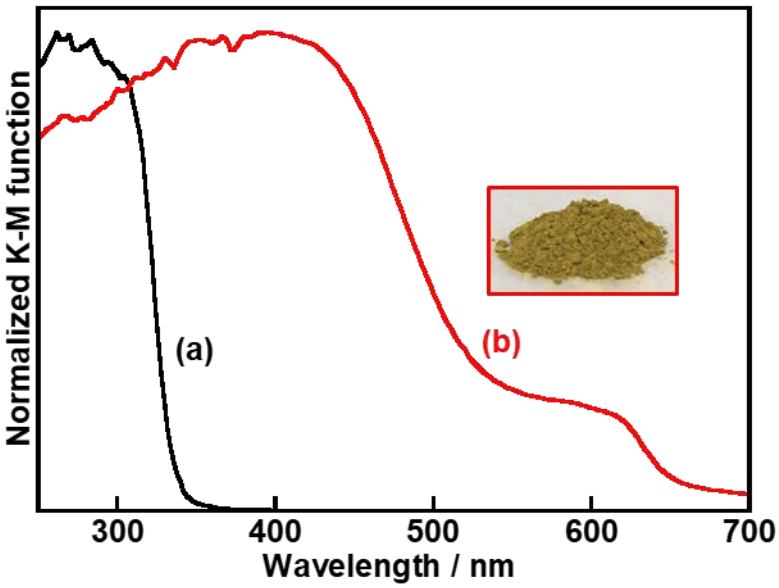

Figure S20. Diffuse reflectance spectra of (a) $Na_2La_2Ti_3O_{10}$ and (b) Cu(I)-$Na_2La_2Ti_3O_{10}$, and a photograph of Cu(I)-$Na_2La_2Ti_3O_{10}$.

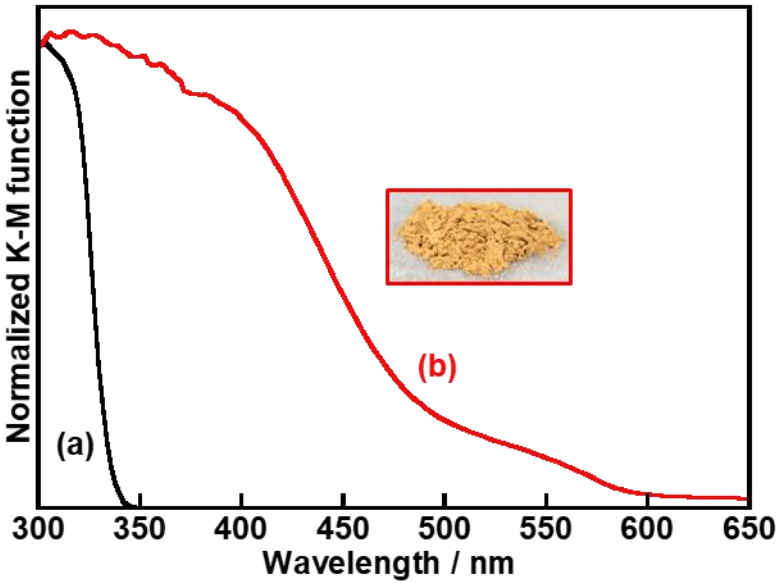

Figure S21. Diffuse reflectance spectra of (a) $Li_2La_2Ti_3O_{10}$ and (b) Cu(I)-$Li_2La_2Ti_3O_{10}$, and a photograph of Cu(I)-$Li_2La_2Ti_3O_{10}$.

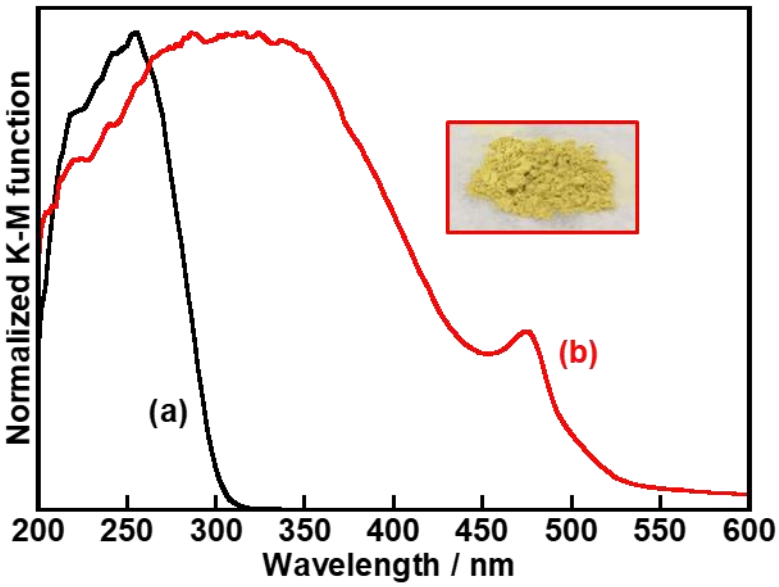

Figure S22. Diffuse reflectance spectra of (a) $K_2CaNaTa_3O_{10}$ and (b) Cu(I)-$K_2CaNaTa_3O_{10}$, and a photograph of Cu(I)-$K_2CaNaTa_3O_{10}$.

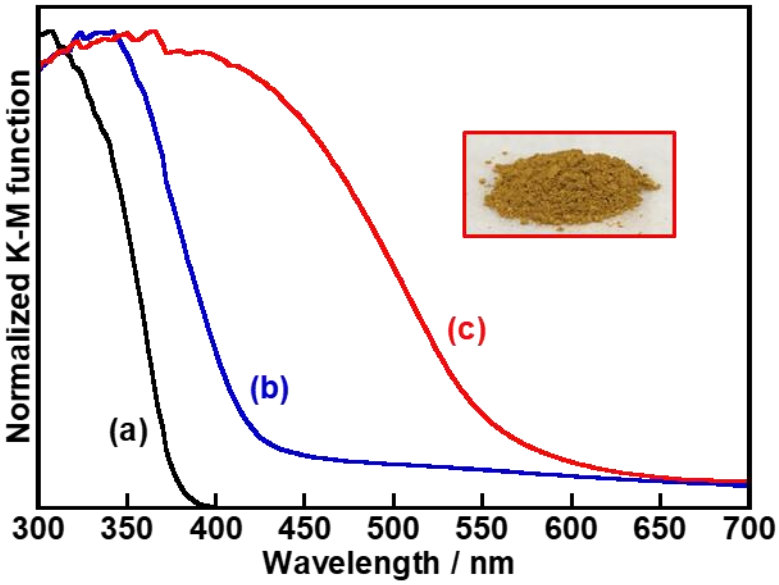

Figure S23. Diffuse reflectance spectra of (a) $K_2CaNaNb_3O_{10}$, (b) Ag(I)-$K_2CaNaNb_3O_{10}$, and (c) Cu(I)-$K_2CaNaNb_3O_{10}$, and a photograph of Cu(I)-$K_2CaNaNb_3O_{10}$.

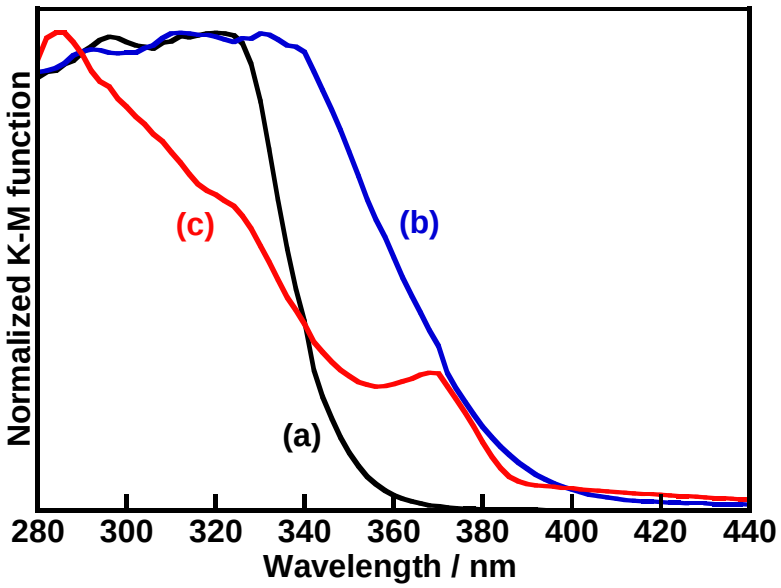

Figure S24. Diffuse reflectance spectra of (a) $KCa_2Nb_3O_{10}$, (b) Ag(I)-$KCa_2Nb_3O_{10}$, and (c) Cu(I)-$KCa_2Nb_3O_{10}$.

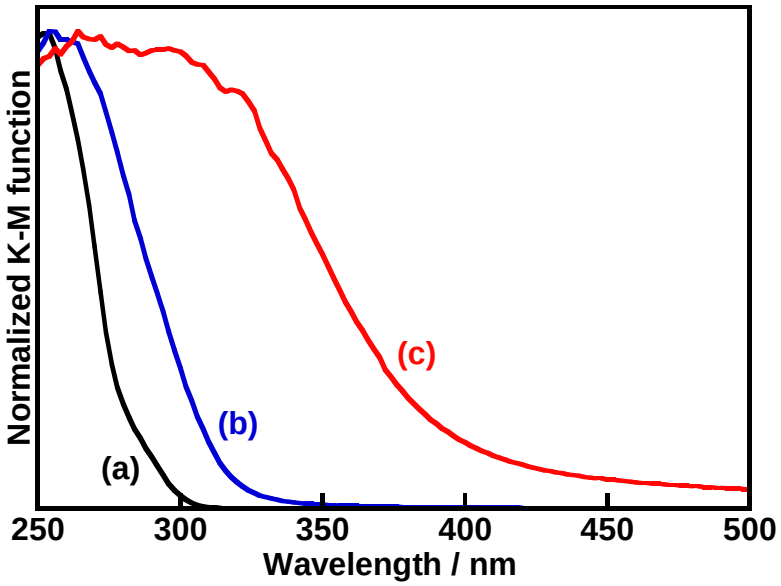

Figure S25. Diffuse reflectance spectra of (a) $CsSr_2Ta_3O_{10}$, (b) Ag(I)-$CsSr_2Ta_3O_{10}$, and (c) Cu(I)-$CsSr_2Ta_3O_{10}$.

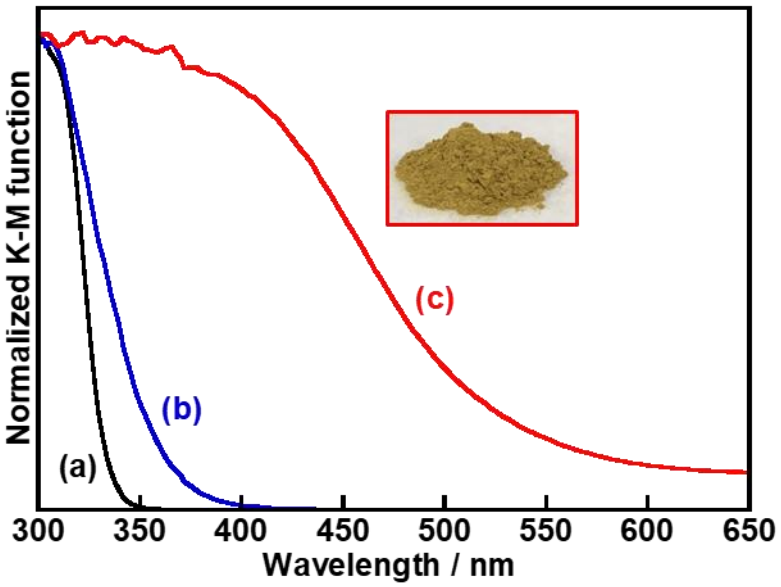

Figure S26. Diffuse reflectance spectra of (a) $CsLa_2Ti_2TaO_{10}$, (b) Ag(I)-$CsLa_2Ti_2TaO_{10}$, and (c) Cu(I)-$CsLa_2Ti_2TaO_{10}$, and a photograph of Cu(I)-$CsLa_2Ti_2TaO_{10}$.

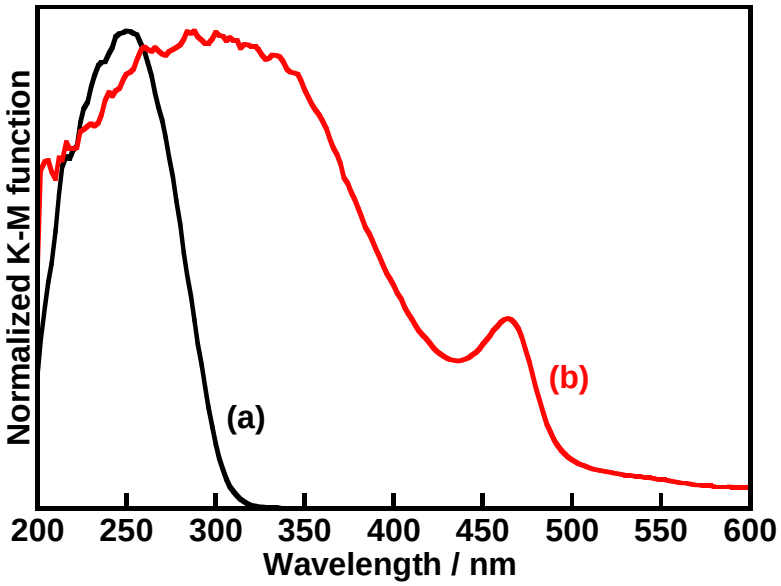

Figure S27. Diffuse reflectance spectra of (a) $K_2La_{2/3}Ta_2O_7$ and (b) Cu(I)-$K_2La_{2/3}Ta_2O_7$.

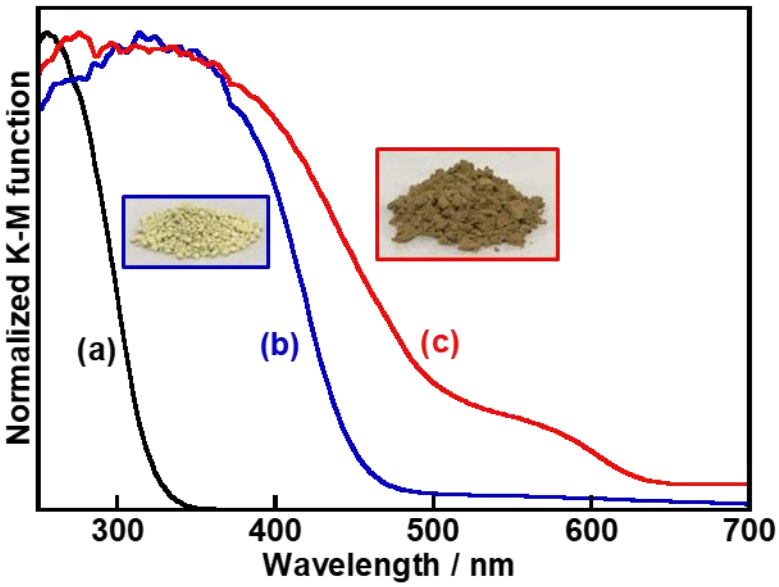

Figure S28. Diffuse reflectance spectra of (a) $K_2SrNb_{0.2}Ta_{1.8}O_7$, (b) Ag(I)-$K_2SrNb_{0.2}Ta_{1.8}O_7$, and (c) Cu(I)-$K_2SrNb_{0.2}Ta_{1.8}O_7$, and photographs of Ag(I)-$K_2SrNb_{0.2}Ta_{1.8}O_7$ (red frame) and Cu(I)-$K_2SrNb_{0.2}Ta_{1.8}O_7$ (blue frame).

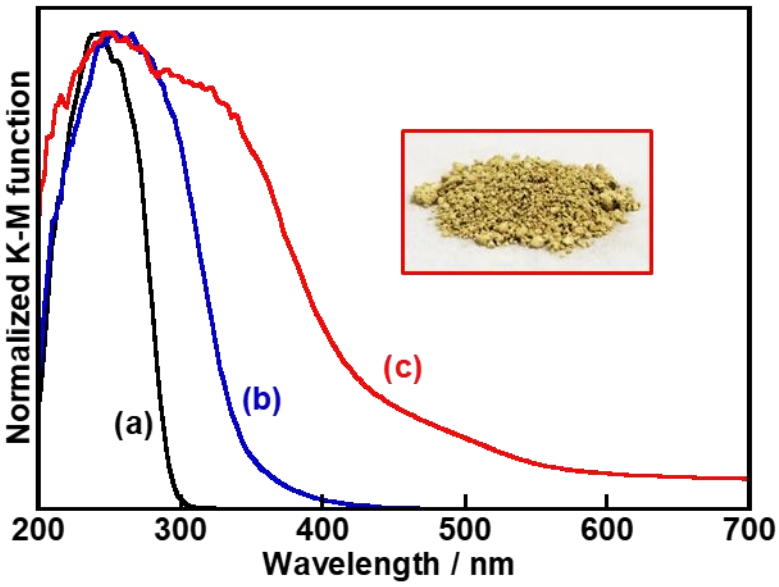

Figure S29. Diffuse reflectance spectra of (a) $KLaTa_2O_7$, (b) Ag(I)-$KLaTa_2O_7$, and (c) Cu(I)-$KLaTa_2O_7$, and a photograph of Cu(I)-$KLaTa_2O_7$.

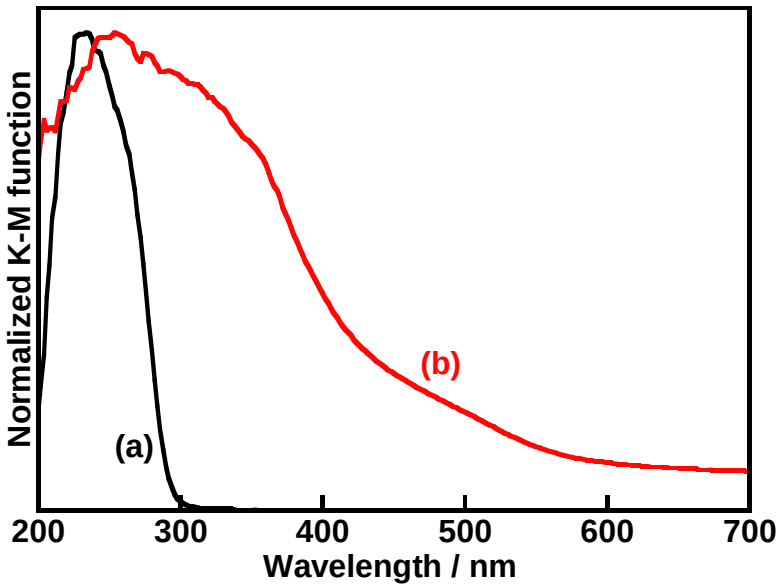

Figure S30. Diffuse reflectance spectra of (a) $RbLaTa_2O_7$ and (b) Cu(I)-$RbLaTa_2O_7$.

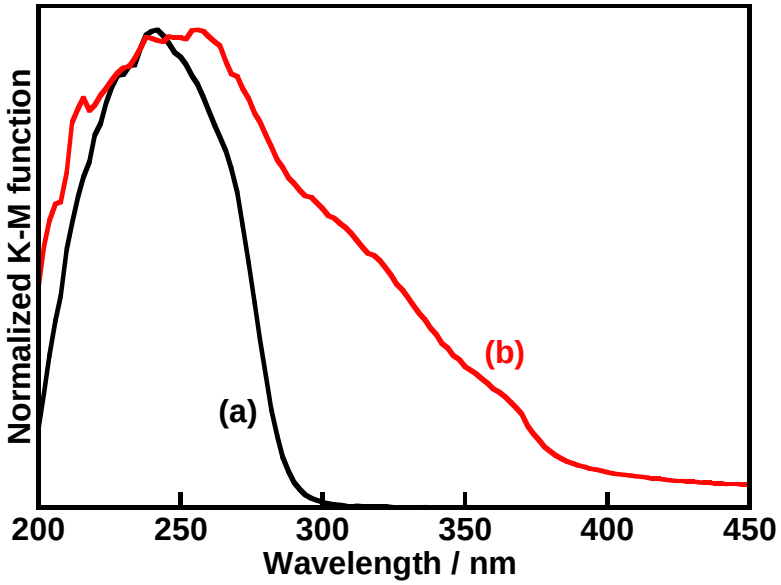

Figure S31. Diffuse reflectance spectra of (a) $LiLaTa_2O_7$ and (b) Cu(I)-$LiLaTa_2O_7$.

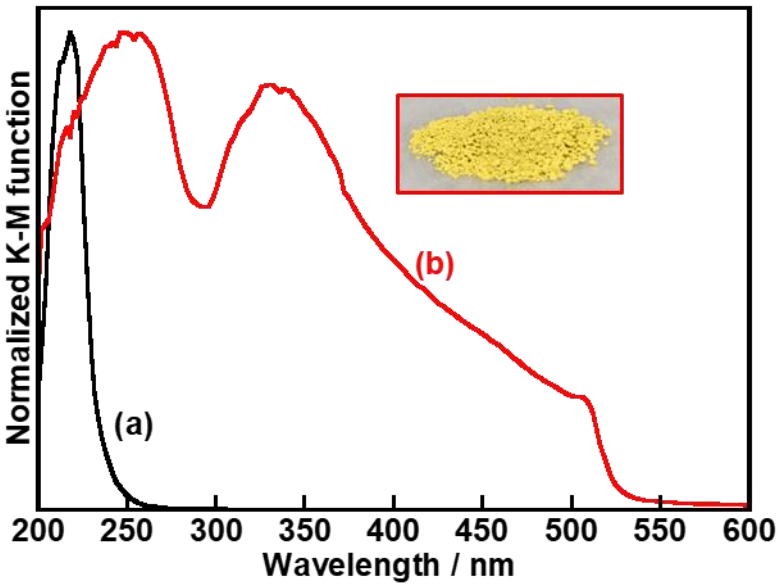

Figure S32. Diffuse reflectance spectra of (a) Li_2SnO_3 and (b) Cu(I)-Li_2SnO_3, and a photograph of Cu(I)-Li_2SnO_3.

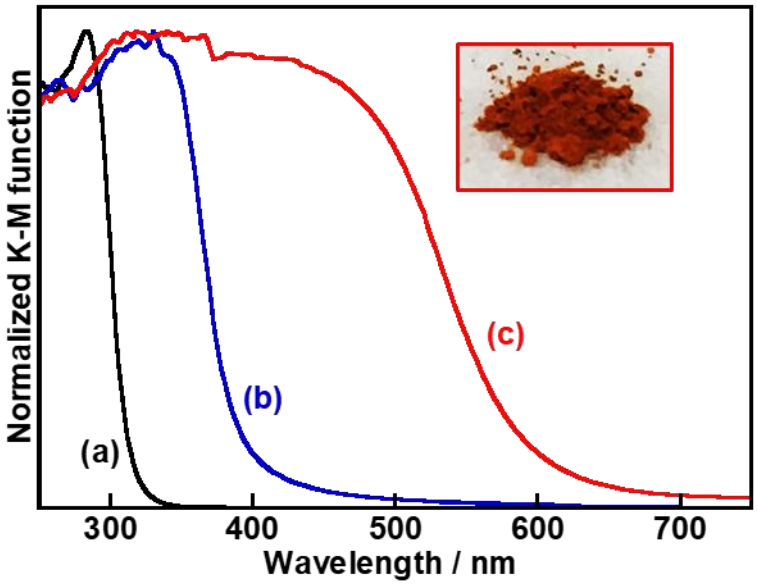

Figure S33. Diffuse reflectance spectra of (a) $K_{0.8}Mg_{0.4}Ti_{1.6}O_4$, (b) Ag(I)-$K_{0.8}Mg_{0.4}Ti_{1.6}O_4$, and (c) Cu(I)-$K_{0.8}Mg_{0.4}Ti_{1.6}O_4$, and a photograph of Cu(I)-$K_{0.8}Mg_{0.4}Ti_{1.6}O_4$.

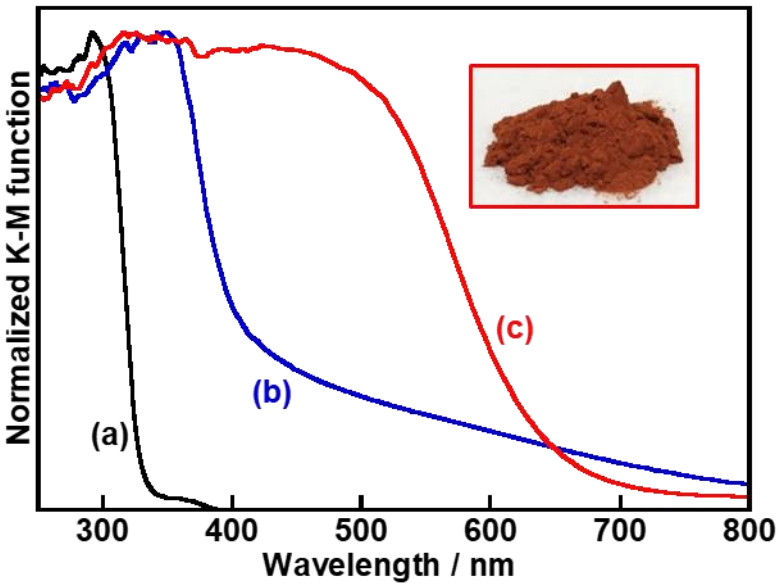

Figure S34. Diffuse reflectance spectra of (a) $K_{0.8}Zn_{0.4}Ti_{1.6}O_4$, (b) Ag(I)-$K_{0.8}Zn_{0.4}Ti_{1.6}O_4$, and (c) Cu(I)-$K_{0.8}Zn_{0.4}Ti_{1.6}O_4$, and a photograph of Cu(I)-$K_{0.8}Zn_{0.4}Ti_{1.6}O_4$.

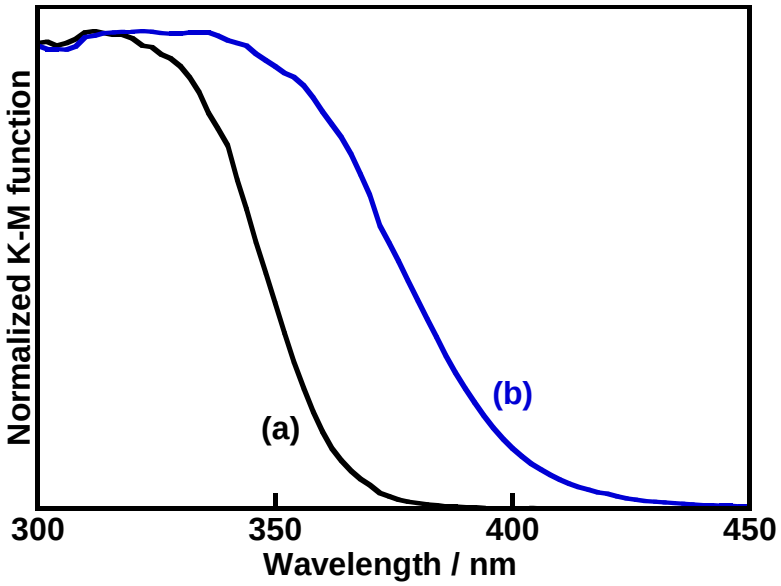

Figure S35. Diffuse reflectance spectra of (a) $KLaNb_2O_7$ and (b) Ag(I)-$KLaNb_2O_7$.

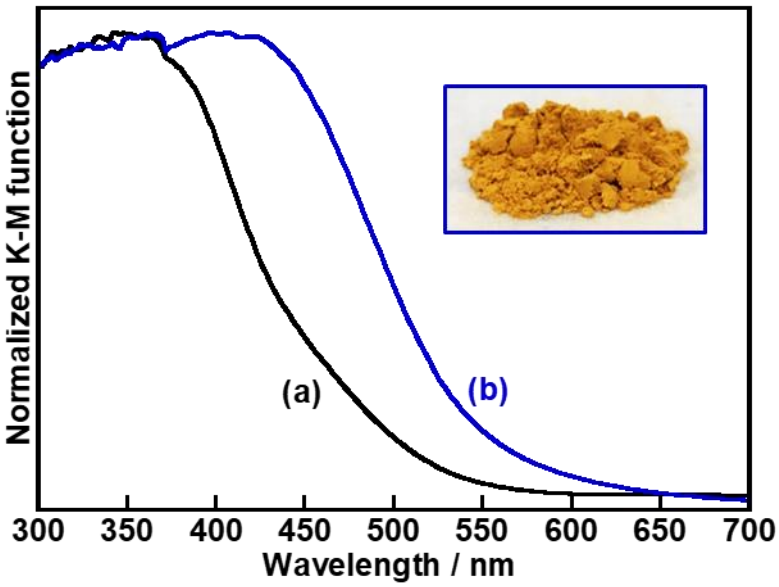

Figure S36. Diffuse reflectance spectra of (a) $LiVWO_6$ and (b) Ag(I)-$LiVWO_6$, and a photograph of Ag(I)-$LiVWO_6$.

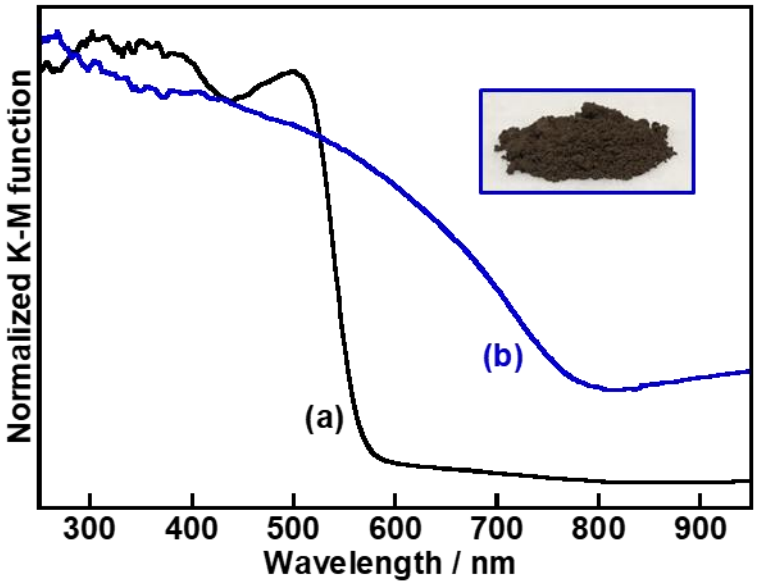

Figure S37. Diffuse reflectance spectra of (a) KV_3O_8 and (b) Ag(I)-KV_3O_8, and a photograph of Ag(I)-KV_3O_8.

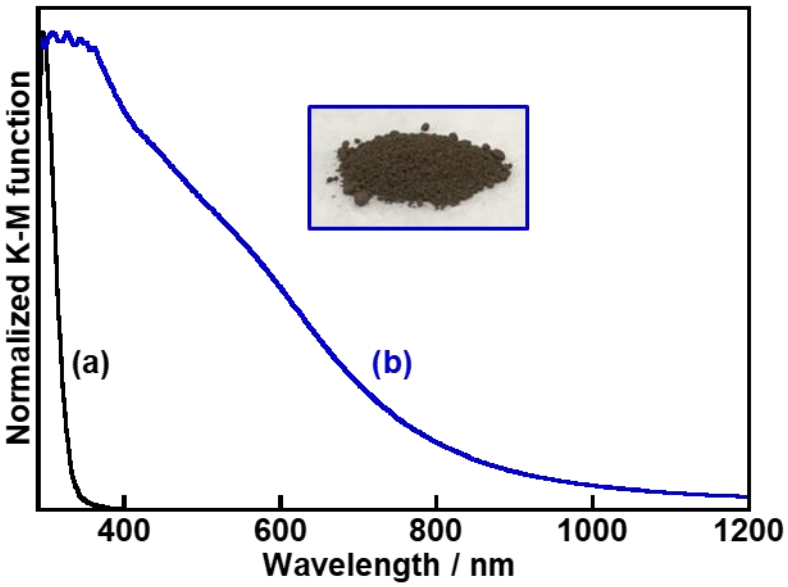

Figure S38. Diffuse reflectance spectra of (a) $K_2Ti_2O_5$ and (b) Ag(I)-$K_2Ti_2O_5$, and a photograph of Ag(I)-$K_2Ti_2O_5$.

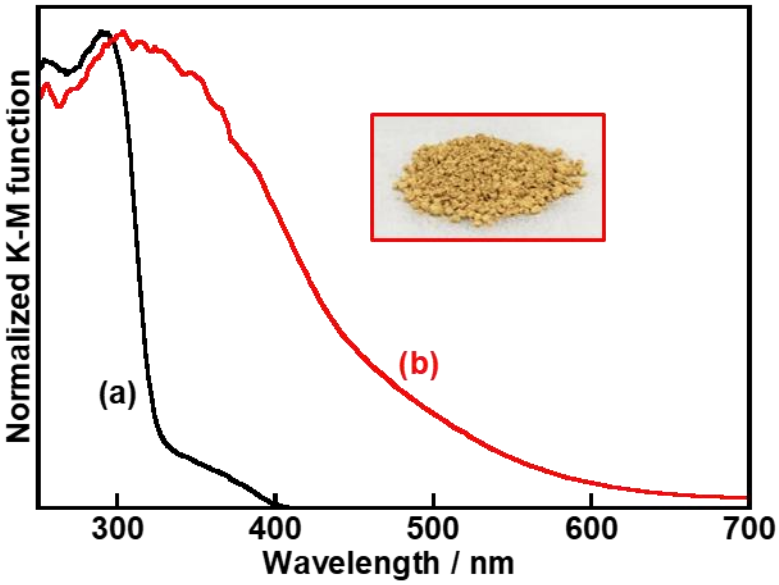

Figure S39. Diffuse reflectance spectra of (a) $CsTi_2NbO_7$ and (b) Cu(I)-$CsTi_2NbO_7$, and a photograph of Cu(I)-$CsTi_2NbO_7$.

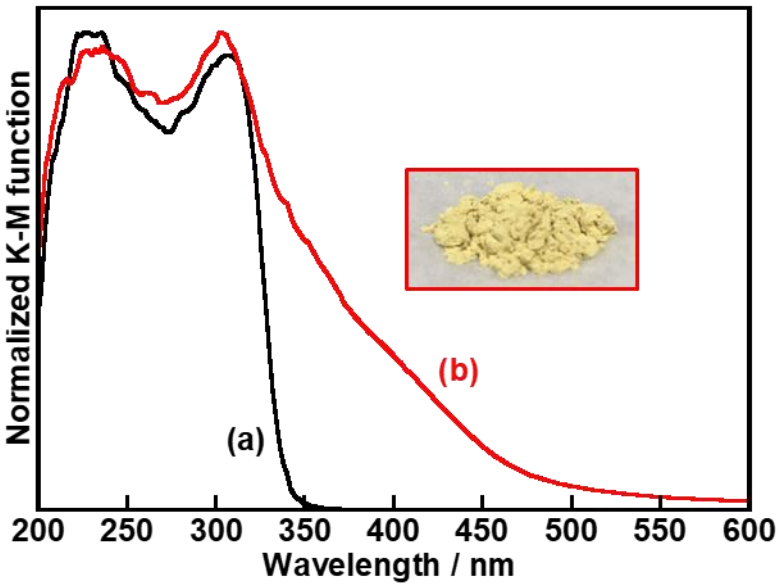

Figure S40. Diffuse reflectance spectra of (a) $Li_2Na_2Ti_6O_{14}$ and (b) Cu(I)-$Li_2Na_2Ti_6O_{14}$, and a photograph of Cu(I)-$Li_2Na_2Ti_6O_{14}$.

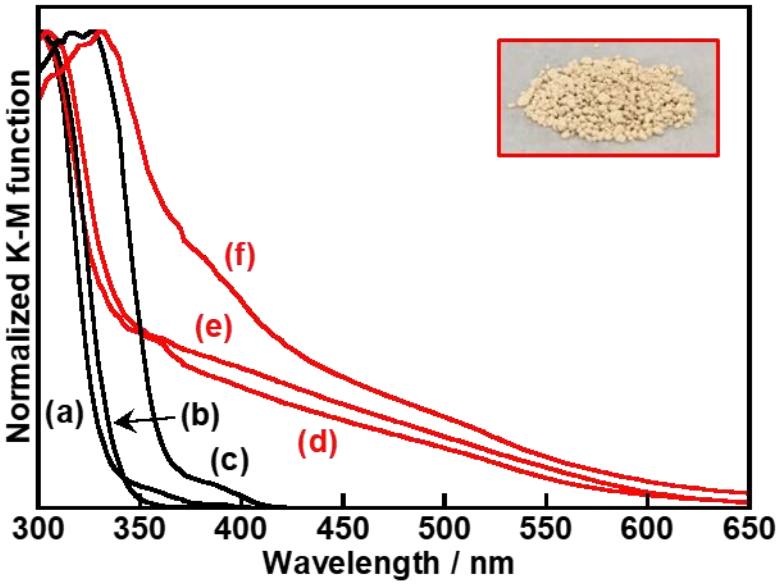

Figure S41. Diffuse reflectance spectra of (a) $Li_2SrTi_6O_{14}$, (b) $Li_2BaTi_6O_{14}$, (c) $Li_2PbTi_6O_{14}$, (d) Cu(I)-$Li_2SrTi_6O_{14}$, (e) Cu(I)-$Li_2BaTi_6O_{14}$, and (f) Cu(I)-$Li_2PbTi_6O_{14}$, and a photograph of Cu(I)-$Li_2SrTi_6O_{14}$.

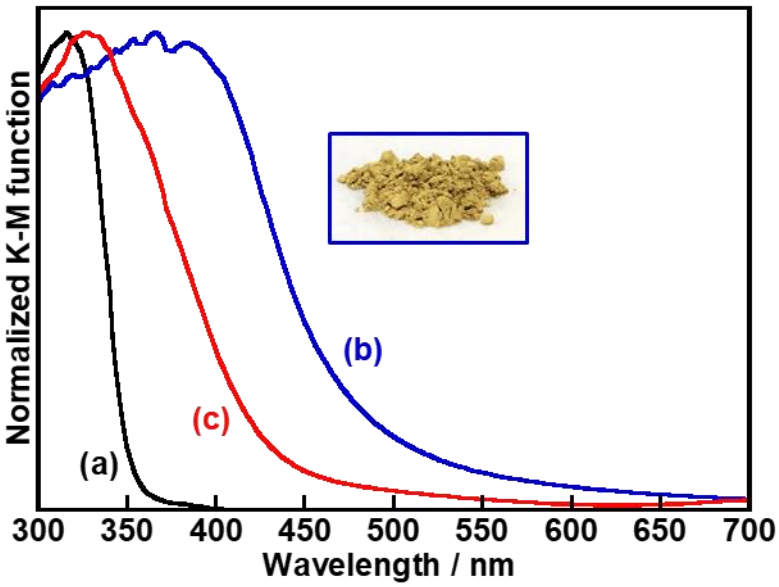

Figure S42. Diffuse reflectance spectra of (a) $Li_2Ti_3O_7$, (b) Ag(I)-$Li_2Ti_3O_7$, and (c) Cu(I)-$Li_2Ti_3O_7$, and a photograph of Ag(I)-$Li_2Ti_3O_7$.

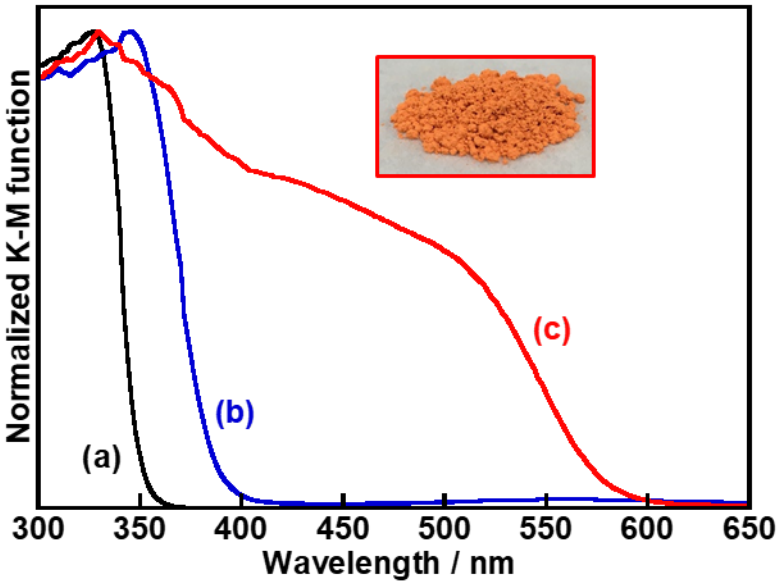

Figure S43. Diffuse reflectance spectra of (a) $Na_2Ti_6O_{13}$, (b) Ag(I)-$Na_2Ti_6O_{13}$, and (c) Cu(I)-$Na_2Ti_6O_{13}$, and a photograph of Cu(I)-$Na_2Ti_6O_{13}$.

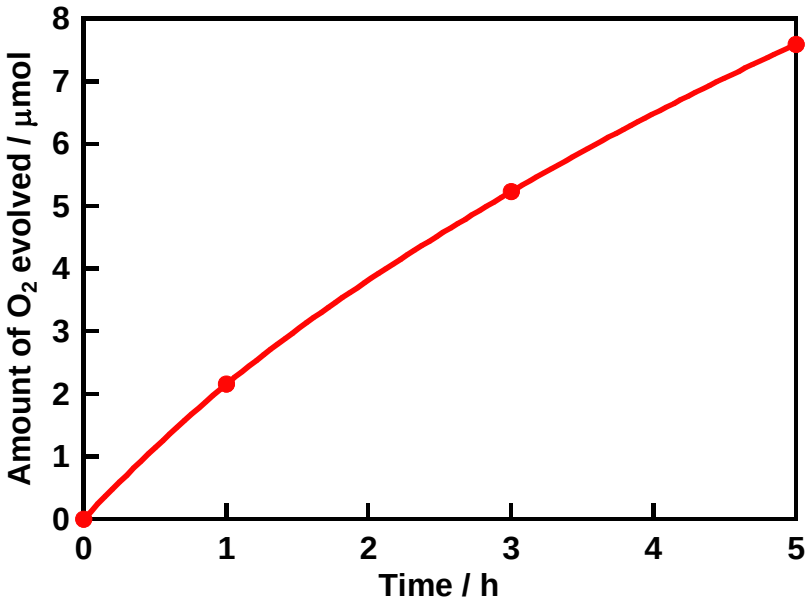

Figure S44. Photocatalytic O_2 evolution over Ag(I)-$K_2SrTa_2O_7$ from an aqueous $AgNO_3$ solution under visible light irradiation. Photocatalyst: 0.5 g, reactant solution: 20 mmol L^{-1} $AgNO_{3\ aq.}$ (120 mL), cell: top-irradiation cell with a Pyrex window, light source: 300 W Xe-arc lamp with a long-pass filter (HOYA: L42).

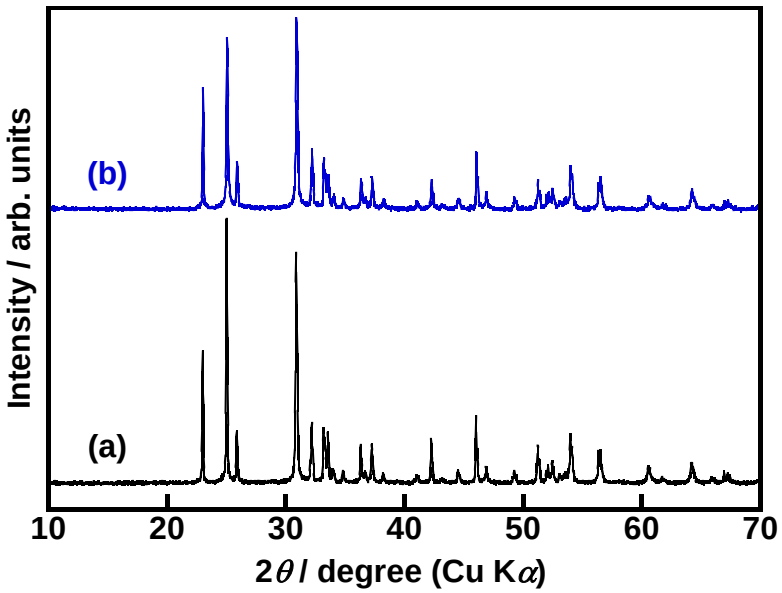

Figure S45. XRD patterns of Ag(I)-$K_2SrTa_2O_7$ (a) before and (b) after photocatalytic O_2 evolution from an aqueous $AgNO_3$ solution under visible light irradiation for 5 h in Figure S44.

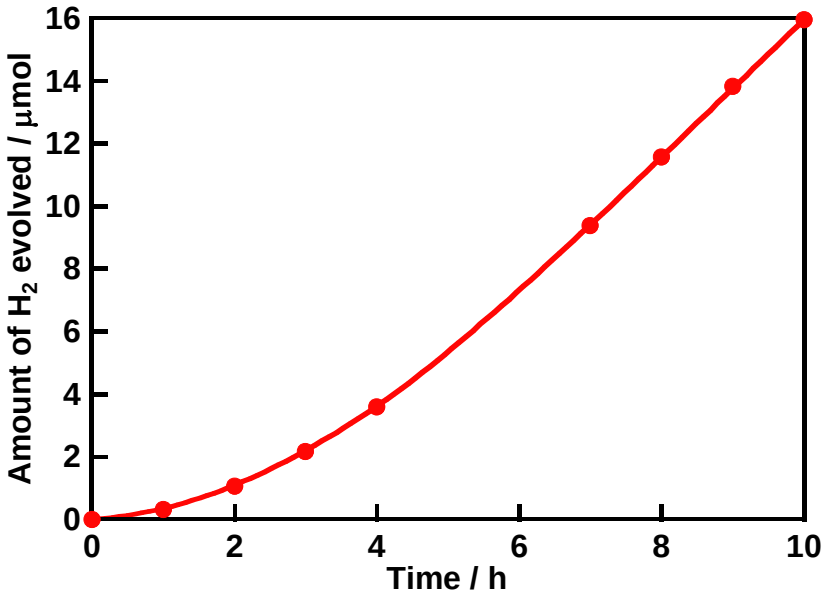

Figure S46. Photocatalytic H_2 evolution over Rh(0.3wt%)/Cu(I)-$Li_2SrTi_6O_{14}$ from an aqueous solution containing sacrificial reagents under visible light irradiation. Photocatalyst: 0.3 g, cocatalyst: photodeposition (*in situ*), reactant solution: 0.5 mol L^{-1} K_2SO_3 + 0.1 mol L^{-1} Na_2S $_{aq.}$ (120 mL), cell: top-irradiation cell with a Pyrex window, light source: 300 W Xe-arc lamp with a long-pass filter (HOYA; Y44).

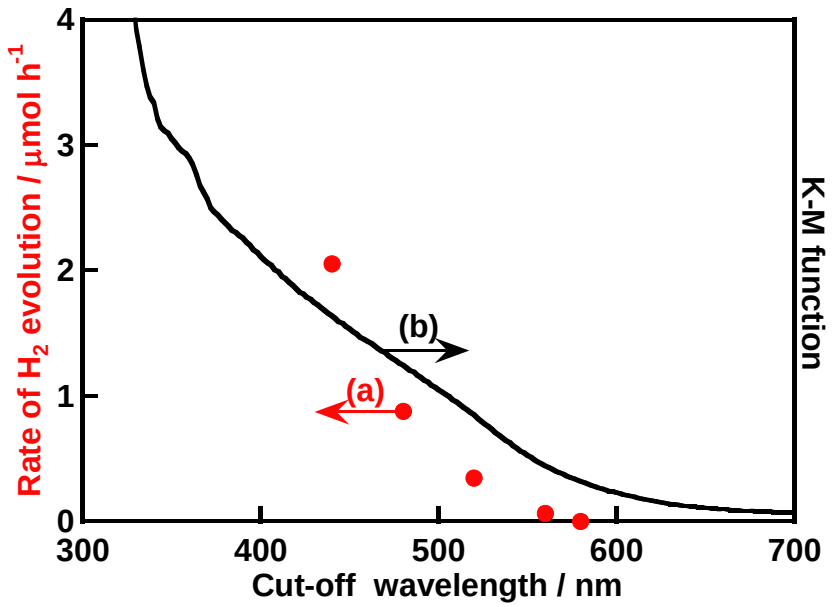

Figure S47. (a) Wavelength dependence of H_2 evolution from an aqueous solution containing sacrificial reagents and (b) diffuse reflectance spectrum of Cu(I)-$Li_2SrTi_6O_{14}$. CuCl-CuI mixture was used as a flux for the synthesis of all Cu(I)-$Li_2SrTi_6O_{14}$. Photocatalyst: 0.3 g, cocatalyst: Rh 1 wt%, reactant solution: 0.5 mol L^{-1} K_2SO_3 + 0.1 mol L^{-1} Na_2S $_{aq.}$ (120 mL), cell: top-irradiation cell with a Pyrex window, light source: 300 W Xe-arc lamp with long-pass filters (HOYA; Y44, Y48, Y52, O56, R58).

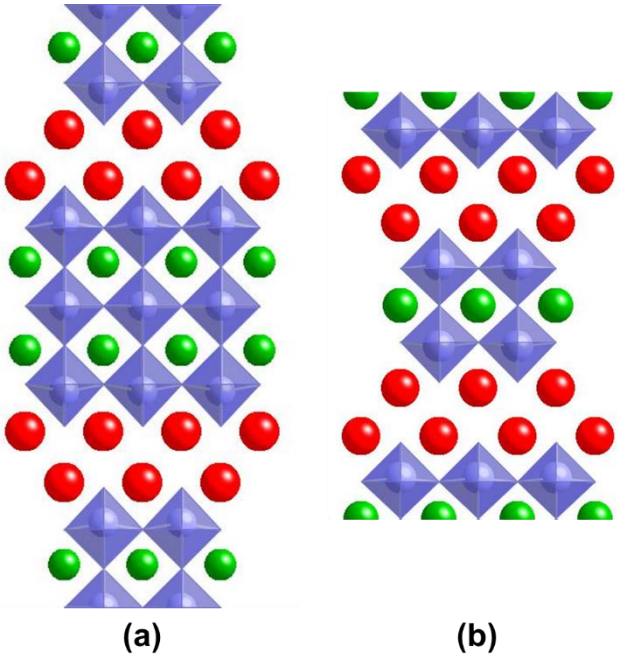

Figure S48. Crystal structures of (a) $K_2La_2Ti_3O_{10}$ and (b) $K_2SrTa_2O_7$ with a Ruddlesden-Popper type layered perovskite structure. Red spheres, green spheres, and blue octahedra indicate K^+, Sr^{2+}/La^{3+}, and TiO_6/TaO_6, respectively.

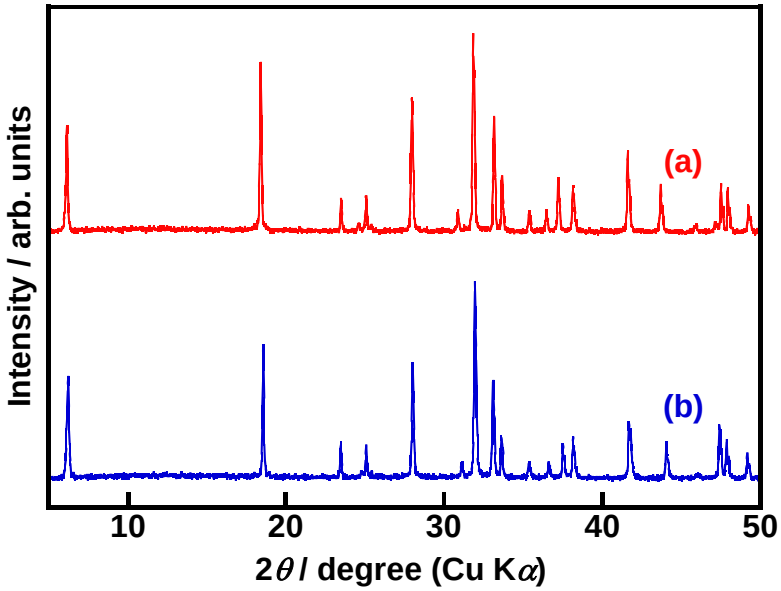

Figure S49. X-ray diffraction patterns of (a) Cu(I)-$K_2La_2Ti_3O_{10}$ and (b) Cu(I)-$Na_2La_2Ti_3O_{10}$. CuCl was used as a flux for the synthesis of Cu(I)-$K_2La_2Ti_3O_{10}$ and Cu(I)-$Na_2La_2Ti_3O_{10}$.

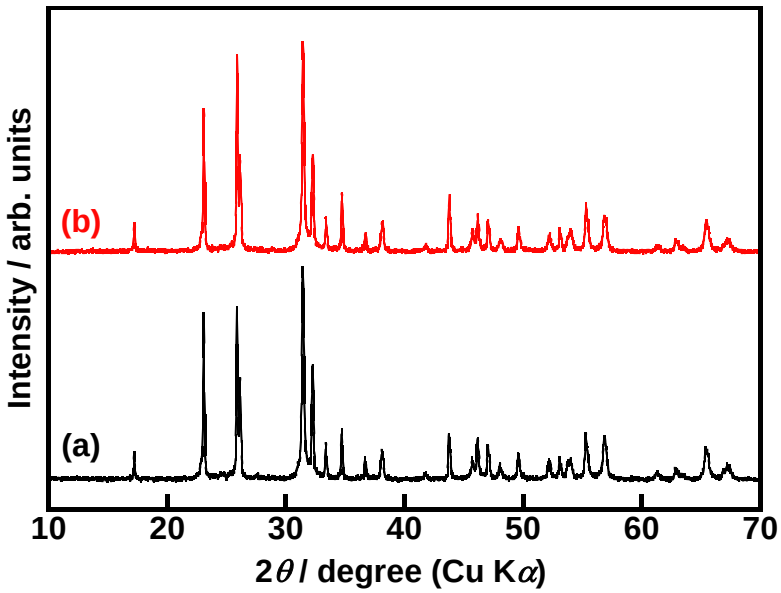

Figure S50. XRD patterns of Cu(I)-$K_2SrTa_2O_7$ (a) before and (b) after photocatalytic H_2 evolution from an aqueous solution containing sacrificial reagents under visible light irradiation for 50 h in Figure 13.

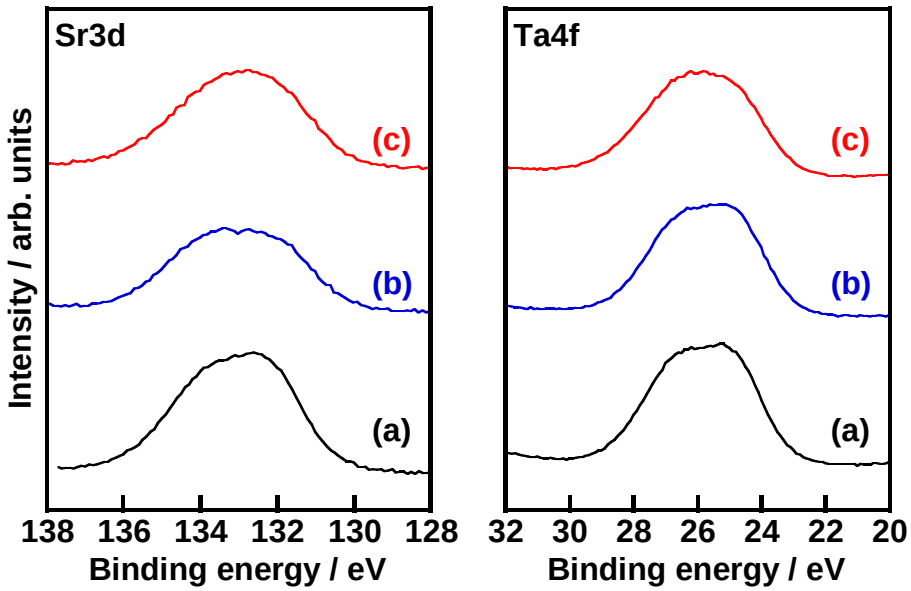

Figure S51. Sr3d and Ta4f XPS spectra of (a) $K_2SrTa_2O_7$, (b) Ag(I)-$K_2SrTa_2O_7$, and (c) Cu(I)-$K_2SrTa_2O_7$. Binding energies of all peaks were calibrated with C1s (284.2 eV).

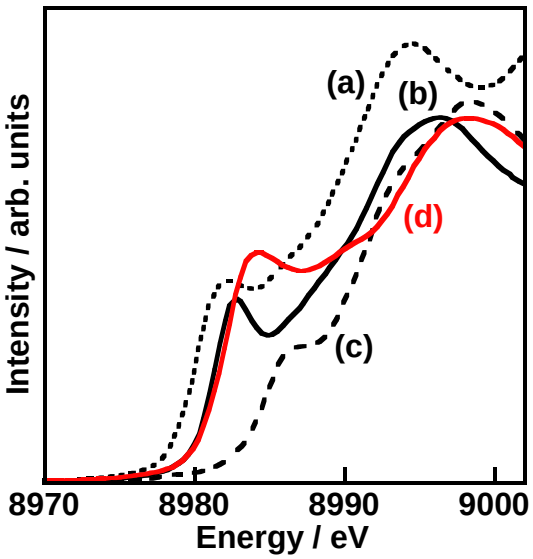

Figure S52. Cu K-edge XANES spectra of (a) Cu foil, (b) Cu_2O, (c) CuO, and (d) Cu(I)-$KLaTa_2O_7$. CuCl was used as a flux for the synthesis of Cu(I)-$KLaTa_2O_7$.

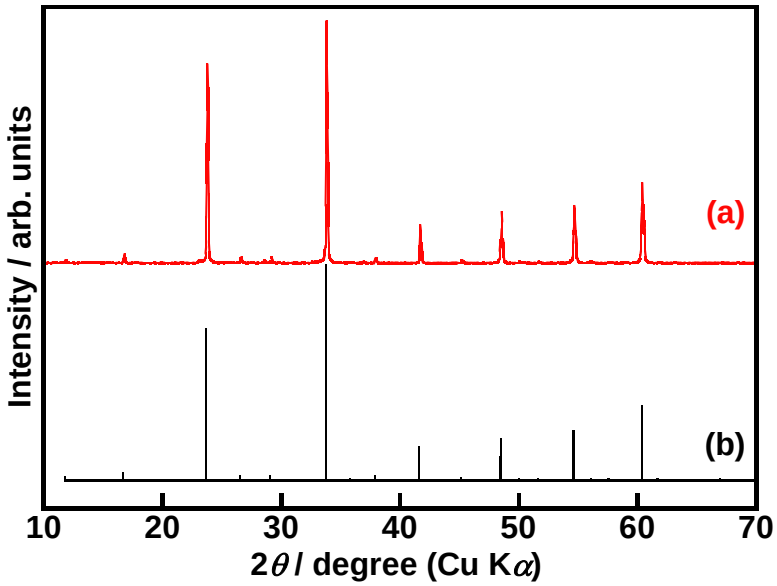

Figure S53. XRD patterns of (a) $CuTa_2O_6$ prepared by a solid state reaction at 1273 K for 20 h in air and (b) $Cu_{1.988}Ta_4O_{12}$ (PDF 1-76-7902).